Hindawi
International Journal of Photoenergy
Volume 2017, Article ID 7686053, 8 pages
https://doi.org/10.1155/2017/7686053

Research Article

Controlled Assembly of Nanorod TiO_2 Crystals via a Sintering Process: Photoanode Properties in Dye-Sensitized Solar Cells

Saeid Vafaei,[1] Kazuhiro Manseki,[2] Soki Horita,[2] Masaki Matsui,[3] and Takashi Sugiura[2]

[1]*Mechanical Engineering Department, Bradley University, 1501 West Bradley Avenue, Peoria, IL 61625, USA*
[2]*Graduate School of Natural Science and Technology, Gifu University, Yanagido, Gifu 501-1193, Japan*
[3]*Faculty of Engineering, Gifu University, Yanagido, Gifu 501-1193, Japan*

Correspondence should be addressed to Kazuhiro Manseki; kmanseki@gifu-u.ac.jp and Takashi Sugiura; tsugiura@gifu-u.ac.jp

Received 15 May 2017; Accepted 5 July 2017; Published 22 October 2017

Academic Editor: Ting Xia

We present for the first time a synthetic method of obtaining 1D TiO_2 nanorods with sintering methods using bundle-shaped 3D rutile TiO_2 particles (3D BR-TiO_2) with the dimensions of around 100 nm. The purpose of this research is (i) to control crystallization of the mixture of two kinds of TiO_2 semiconductor nanocrystals, that is, 3D BR-TiO_2 and spherical anatase TiO_2 (SA-TiO_2) on FTO substrate via sintering process and (ii) to establish a new method to create photoanodes in dye-sensitized solar cells (DSSCs). In addition, we focus on the preparation of low-cost and environmentally friendly titania electrode by adopting the "water-based" nanofluids. Our results provide useful guidance on how to improve the photovoltaic performance by reshaping the numerous 3D TiO_2 particles to 1D TiO_2-based electrodes with sintering technique.

1. Introduction

Organic molecular-based optoelectronic devices have been extensively studied over the last decade, such as in electroluminescent (EL) displays and photovoltaics [1]. In particular, low-cost fabrication is one of the fundamental issues in order to realize a large-scale commercial production. In this regard, a solution processibility of these devices has significant advantages over inorganic ones that require a high-cost vacuum process. Among many emerging technologies, dye-sensitized solar cells (DSSCs) represent opportunities for the creation of many advanced materials and device structures both for indoor and outdoor applications. Grätzel's group for the first time demonstrated the use of highly dispersed TiO_2 nanoparticles as anode materials for high-efficiency DSSCs [2]. The synthesis of highly crystallized TiO_2 nanoparticles is generally required in order to develop high-performance photoelectrode materials in DSSCs [3]. Besides, it is necessary to engineer the porous layer of deposited TiO_2 nanoparticles to (a) enhance the monolayer dye adsorption to the surface of TiO_2 nanoparticles, (b) efficiently collect the generated electrons and conduct them out, and (c) suppress the recombination phenomenon to enable efficient electron transport inside TiO_2 films which plays a crucial role in the solar cell's performance. A number of investigations have demonstrated how DSSCs' performance will be affected by characteristics of TiO_2 nanoparticles; many groups have shown the better electron transport of 1D morphologies of TiO_2 particles over nanoparticulate materials [4].

So far, most of the 1D TiO_2 particles including nanowires, nanotubes, and nanorods have been synthesized by a bottom-up method via wet-chemical approach such as hydrothermal reactions and anodic electrodeposition of suitable Ti(IV) precursors [5, 6]. We present for the first time an alternative synthetic method of obtaining 1D TiO_2 nanorods with sintering methods using bundle-shaped 3D rutile TiO_2 particles (BR-TiO_2) with the dimensions of around 100 nm (Figure 1). Interestingly, it was found that the cocrystallization with tiny spherical anatase TiO_2 crystals (SA-TiO_2)

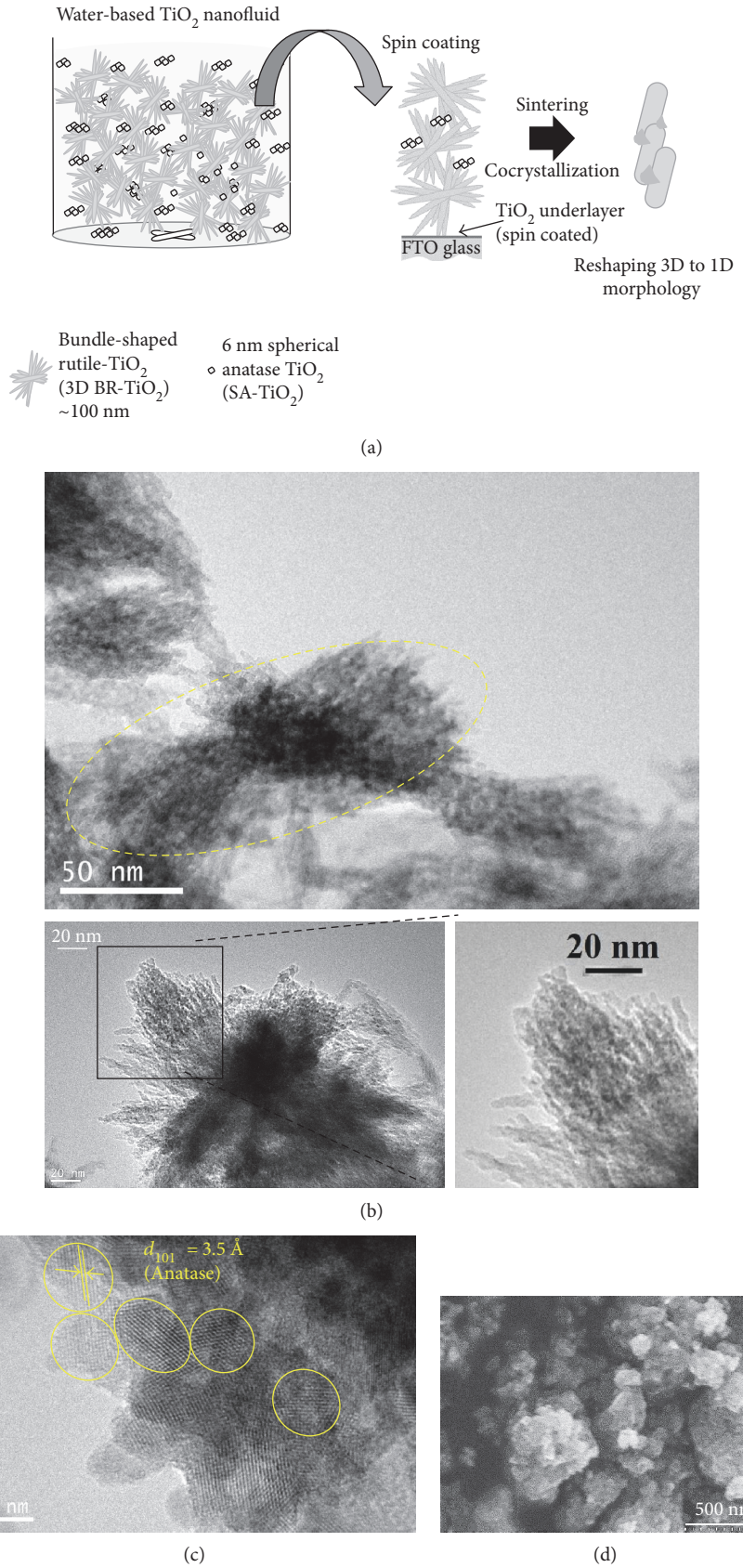

Figure 1: (a) Schematics of BR-TiO_2 and SA-TiO_2 deposited on FTO substrate above the sublayer and subsequent sintering process. (b) TEM images of BR-TiO_2. (c) A TEM image of SA-TiO_2. (d) A SEM image of SA-TiO_2.

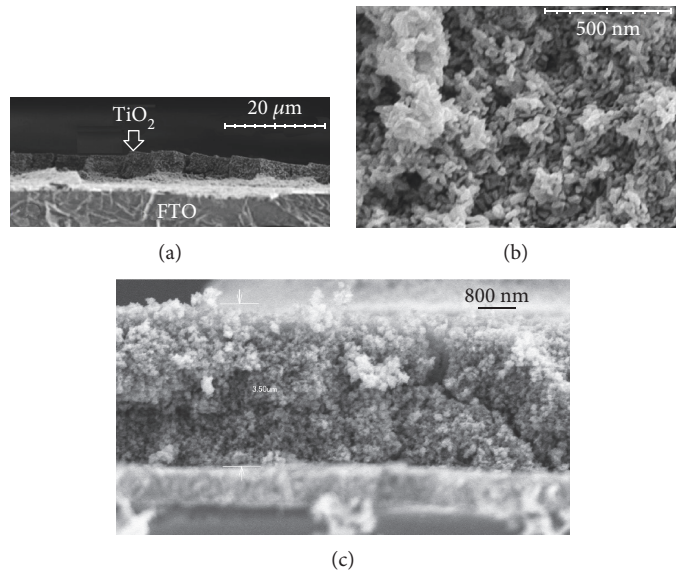

Figure 2: SEM images of the porous layer of deposited BR-TiO_2 particles (33 wt%) on FTO substrate, after sintering. (a) A cross-sectional image of 5 μm thick TiO_2 film. (b) Top side image. (c) A SEM image of 3.5 μm thick TiO_2 film before sintering is shown.

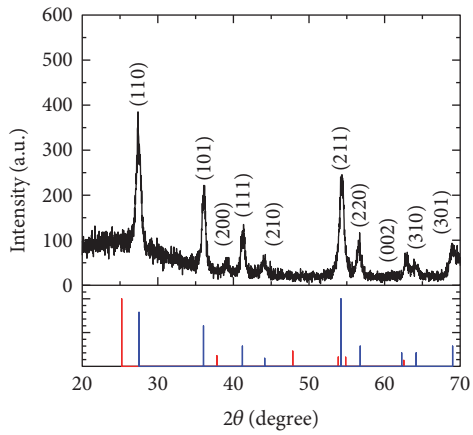

Figure 3: Powder XRD pattern of sintered BR-TiO_2. The concentration of TiO_2 particles: 33 wt%. Blue lines indicate the database values for rutile TiO_2 (PDF: 00-001-1292) and red for anatase TiO_2 (PDF: 00-021-1272).

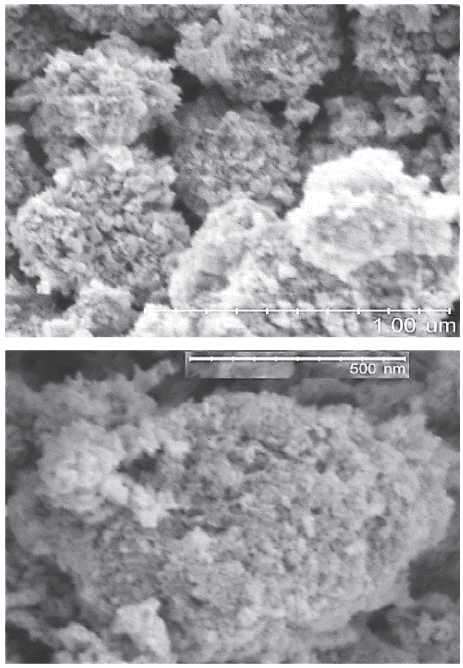

Figure 4: SEM images of the TiO_2 film after sintering. The TiO_2 nanofluid was spread on substrate, using spin coating method. The concentrations of SA-TiO_2 and BR-TiO_2 were, respectively, 20 wt% and 20 wt%.

produced better photoanode performance, that is, improved light-to-electricity conversion efficiency in DSSCs.

There are several cost analyses of DSSCs that have shown a high material cost including transparent conducting glasses, dye molecules, and TiO_2 pastes (precursors as photoanodes) [7]. Therefore, we also focused on the preparation of the low-cost and environmentally friendly titania precursors for creating porous TiO_2 electrodes in DSSCs by the development of "water-based" nanofluids. Here, we combined a standard metal-free indoline dye molecule, D205, as a sensitizer with the newly processed TiO_2 anodes in DSSCs, since the light absorption by such organic dyes can cover a wide range of visible light (with high molar extinction coefficient). Accordingly, the porous TiO_2 semiconductor film with indoline dyes can significantly reduce the TiO_2 thickness, leading to the reduced recombination reactions at the material interface of dyes and electrolytes in DSSCs. We report here the design and preparation of TiO_2 photoelectrode films as a generalized method to develop 1D morphology metal oxides using a sintering method. In addition, a preliminary assessment of the photoanode performance of DSSCs is provided by the creation of cocrystallized TiO_2 assembly using two different TiO_2 particles.

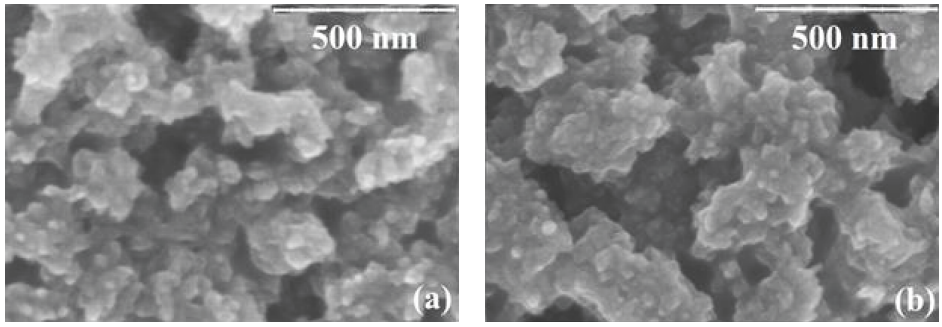

(a) (b)

Figure 5: SEM images of the surface of TiO_2 nanoparticle porous layers made by different nanoparticle concentrations, after successive sintering. The nanoparticles deposited, using spin coating method, (a) 50 wt% SA-TiO_2 (b) 85 wt% SA-TiO_2.

2. Experimental

A solar cell has several main elements, including FTO substrate, dye molecules, electrolytes, and counter electrodes. The main components of the dye solar cells have explained briefly as follows.

2.1. Substrate. F-doped SnO_2-coated glass substrates (FTO, 13Ω/sq.) were used to prepare dyed TiO_2 electrodes. A mixture solution of 8 ml ethanol (99.5%), 0.07 g HCl (35–37%), and 0.71 g titanium tetraisopropoxide (95%) was deposited on the top of FTO by a spin coating. The purpose of the coating was to form a sublayer for deposited TiO_2 nanofluids. The coated layer would enhance the wettability and stability of deposited BR-TiO_2 particles. The coating was conducted by using two-step method: step one, the substrate was coated using 1500 rpm for 30 sec, and step two, the substrate was dried, using 1000 rpm for 60 sec. Figure 1(a) shows the deposited BR-TiO_2 nanoparticles on top of FTO substrate.

2.2. Deposited Porous Layer of TiO_2 Nanoparticles. We have recently reported on synthesis and crystal growth mechanism of BR-TiO_2 [8]. Practically, the BR-TiO_2 were mixed with deionized water to produce nanofluids with a concentration of 40 wt%. It was observed that BR-TiO_2 were dispersed uniformly inside the water which provide low-cost and environmentally friendly nanofluid. To see the effects of the combination of particles with different geometries, small anatase nanoparticles with the average crystallite size of 6 nm (commercial, AMT100, TAYKA, represented as A-TiO_2) (Figures 1(c) and 1(d)) were mixed with the BR-TiO_2. The mass percentage of SA-TiO_2 ($m_A/m_A + m_{NR}$) was 35%, 50%, and 85%. m_A is the mass of SA-TiO_2, and m_{NR} is the mass of BR-TiO_2. Figure 1(b) shows the TEM image of BR-TiO_2.

The nanoparticles were mixed uniformly, using ultrasonicator and rotational agitator. To form a layer of TiO_2 nanoparticles on substrate, a layer of nanofluid was deposited on the coated FTO substrate, using spin coating technique. The thickness of deposited nanofluid was controlled by speed and period of spin coating. In this study, two-step and one-step strategies were used to coat the FTO substrate. (Two steps: substrate was coated, using 1500 rpm for 30 sec, and then it dried at 1000 rpm for 60 sec. One step: substrate was coated and dried, using 500 rpm for 250 sec.) Surface wettability has an important role on thickness of nanofluid on substrate [9–16]. The thickness of nanofluid decreases, as affinity of liquid for substrate increases. The base liquid, surfactant, concentration, and characteristics of nanoparticle have a significant role on surface wettability. After depositing nanoparticles, the sintering method was applied to join the nanoparticles together and form tiny porous layer of deposited nanoparticles on FTO substrate. Typically, the deposited nanoparticles were sintered at 500°C for 60 minutes, using an oven. The temperature was raised with a speed of 100 rpm per hour to achieve 500°C. Similarly, the temperature was reduced to ambient temperature.

2.3. Device Assembly. The deposited TiO_2 porous layer on FTO substrate was immersed in the D205 dye solution. The solvent was the combination of acetonitrile (super dehydrated) and *t*-butyl alcohol with a volume ratio of 1 : 1. The solution was kept in the dark at 25°C. The dye adsorption time for D205 dye was 4 hours, and dye concentration was 0.2 mM. Chenodeoxycholic acid was used as a coadsorbent (0.4 mM). Pt-sputtered FTO glasses were used as counter electrodes. The dyed electrode and counter electrode were assembled into a sandwich-type cell. The regeneration of the oxidized dye (formed by light irradiation) is possible by accepting electrons from an electrolyte (a redox system). The electrolyte solution was a combination of 0.6 M 1,2-dimethyl-3-propylimidazolium iodide, 0.1 M LiI, 0.05 M I_2, and 0.05 M 4-*t*-butylpyridine using 3-methoxypropionitrile as a solvent. The electrolyte was filled into the assembled cell with a vacuum backfilling method [17].

2.4. Evaluation of Electrode Films and Device Performance. Structures of porous TiO_2 electrodes were characterized by scanning electron microscopy (SEM) using HITACHI S-4800, HITACHI SU-8000, KEYENCE VE-7800, and X-ray diffraction (Rint-Ultma/PC). Film thickness was estimated with KEYENCE VE-7800. The performance of photon-to-electricity conversions was examined by fabricating DSSCs in a similar manner to the reported method [18]. Photocurrent-voltage curves were obtained under AM 1.5-simulated sunlight (100 mW/cm^2) by using Yamashita Denso YSS-80A

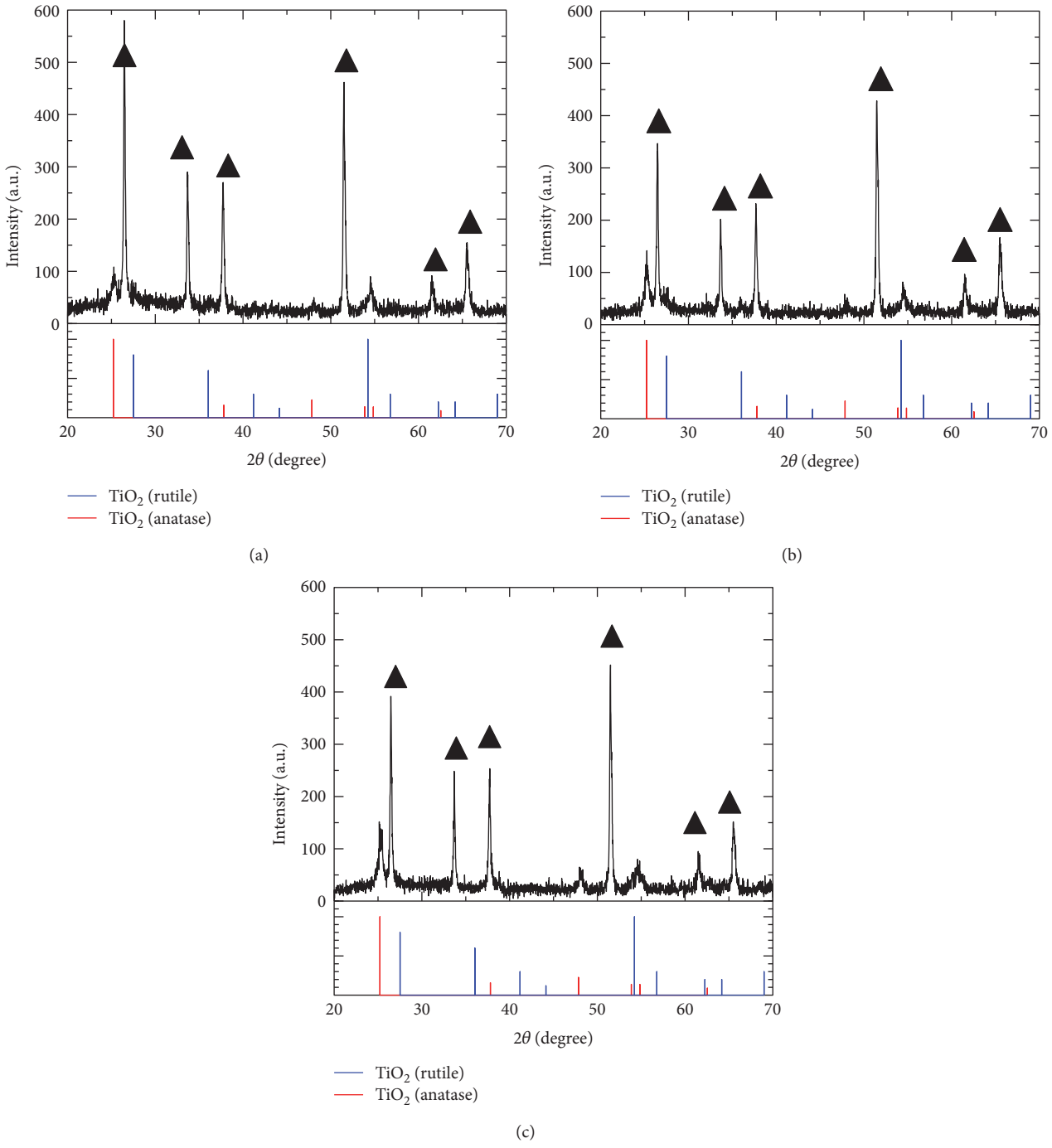

FIGURE 6: XRD pattern of mixed TiO_2 particles of (a) 35 wt%, (b) 50 wt%, and (c) 85 wt% after sintering. The measurements were performed using TiO_2 films deposited on FTO substrates. The triangle indicates SnO_2 peaks coming from the substrate.

with a black mask (4 mm × 5 mm) regulated for the active area of the device.

3. Results and Discussion

The BR-TiO_2 were mixed with deionized water to produce TiO_2 nanofluid. The TiO_2 nanofluid was dispersed on substrate, using a spin coating technique. The deposited nanoparticles were sintered to enhance the electron transport in the semiconductor, using an oven. Figure 2 shows the cross-sectional and top images of the porous layer of deposited BR-TiO_2 nanoparticles on FTO surface (33 wt%) after sintering. The well-dispersed feature of the precursor solution produced a homogenous film. As shown in Figures 1(b), 2(b), and 2(c), TEM and SEM images revealed that the sintering of the TiO_2 precursor film consisting of only larger TiO_2 particles with the size of around 100 nm converts the original bundle-shaped morphology to 1D nanorods as a result of the sintering process. Upon sintering, the nanoscale surface (nanowire structure with ~5 nm width) as can be seen in a TEM image

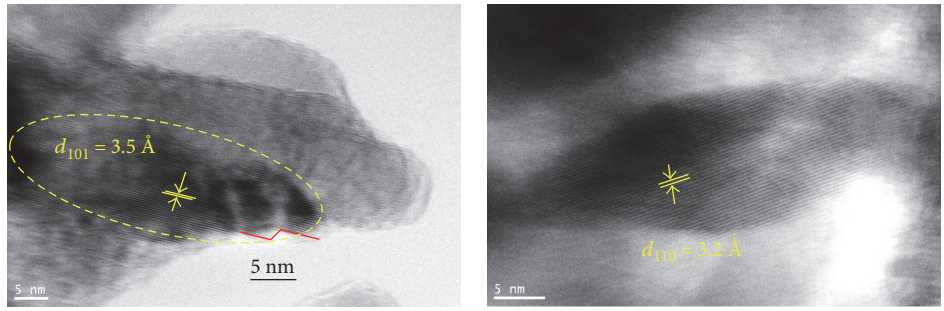

(a) (b)

Figure 7: (a) HR-TEM image showing the lattice spacing of anatase TiO_2 crystals (yellow lines) formed by successive sintering. The red line shows zigzag-shaped edges of an anatase phase TiO_2 exposing 101 crystal facets. (b) A TEM image showing the formation of 1D nanorod.

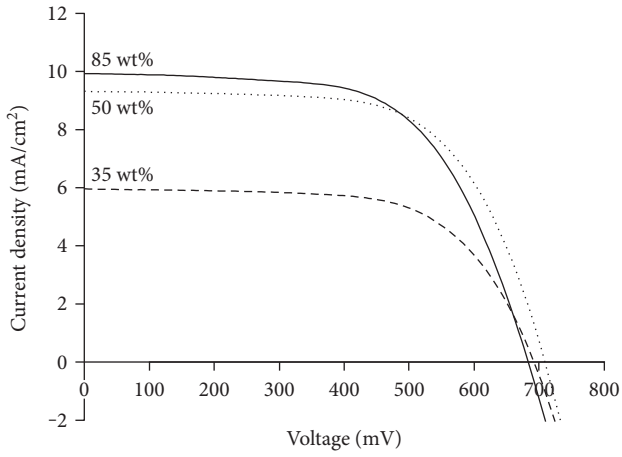

Figure 8: Variation of photocurrent as a function of photovoltage of DSSCs using water-based TiO_2 nanofluids with 60 wt% water and 40 wt% mixture of BR-TiO_2 and SA-TiO_2. Concentration of SA-TiO_2 was 35 wt%, 50 wt%, and 85 wt%. The solar cells was tested under simulated 1 sunlight.

of Figure 1(b) reacts with each other and a significant reduction of micropores in the surface of the original BR-TiO_2 takes place resulting in the reshaped 1D-shaped nanorods. In order to characterize the obtained particles, X-ray diffraction (XRD) measurement which is often used to analyze polycrystalline compounds was performed. The powder XRD pattern of the same sample (see Figure 3) matches well with the database of rutile TiO_2 crystals. Previously, we reported that as-prepared BR-TiO_2 has a rutile crystal phase. Accordingly, it was found that the rutile crystal type of TiO_2 is retained after sintering.

We anticipated that such a surface reactivity would enhance the interparticle's connection of BR-TiO_2, especially when BR-TiO_2 are surrounded by small SA-TiO_2. It is plausible that the SA-TiO_2 nanoparticles (anatase) have a tendency to agglomerate and produce bigger clustered particles in the nanofluid. Figure 4 shows the porosity of semiconductor (concentrations of SA-TiO_2 and BR-TiO_2 were 20 wt%) after sintering. It was observed that SA-TiO_2 clusters at the surface of BR-TiO_2 and produces larger crystals after sintering. This simultaneously results in the joining of TiO_2 interparticles in the film. Figure 5 shows the porosity of semiconductor for different concentration of SA-TiO_2. After sintering, SEM images of TiO_2 films (porous photoanodes) in Figure 5 suggest that as nanoparticle concentration increases, the possibility of nanoparticle collision increases and consequently nanoparticles have more chance to agglomerate and form bigger clusters on substrate. Similar phenomenon has been observed during nanofluid pool and flow boiling [19–22].

Figure 6 shows XRD pattern of mixed TiO_2 particles deposited on FTO substrates. XRD pattern shows that more intense peaks at around 25° (2θ) assigned to added SA-TiO_2 are observed with increasing the TiO_2 concentration. From these peaks, we estimated crystallite sizes of the anatase TiO_2 particles using the Scherrer equation, $D = K\lambda/\beta\cos\theta$, where a peak width β is inversely proportional to crystallite size (D). The values of K, λ, and θ indicate Scherrer constant (=0.90), X-ray wavelength (=1.54 Å), and Bragg angle, respectively. It turned out that the values of crystallite sizes of the anatase TiO_2 particles are 11 nm, 17 nm, and 19 nm for 35 wt%, 50 wt%, and 85 wt%. HR-TEM analysis was performed for the sintered film to investigate the crystallization of anatase TiO_2. As shown in Figure 7, the 50 wt% sintered sample indicated the lattice fringe of $d = 3.5$ Å, which is assigned to an anatase phase of TiO_2. It was found that sintering process of clustered SA-TiO_2 produces larger anatase crystals on the rod-shaped particle, as suggested from TEM image in Figure 7(a). The TEM image in Figure 7(b) shows the formation of 1D nanorod TiO_2 due to a sintering process. Importantly, it is postulated that the number of grain boundary of sintered rutile BR-TiO_2 particles is reduced by the addition of SA-TiO_2 to form chain-like TiO_2 crystals in the TiO_2 film as shown in Figure 6.

In this study, the effects of nanoparticle concentration were investigated on performance of deposited TiO_2 semiconductor by comparing photovoltaic performance of solar cells. Figure 8 shows typical I–V curves, and Table 1 summarizes the photovoltaic performance of devices made by different nanofluid concentrations, exhibiting TiO_2 thickness, short-circuit current density J_{sc} (mA/cm^2), open-circuit voltage V_{oc} (mV), FF, and percentage of photovoltaic performance. Solar cells were made, using coated FTO substrate and D205 dye which is a well-known indoline sensitizer.

SA-TiO_2 were mixed with BR-TiO_2 to prepare nanofluids with 40 wt% TiO_2 and 60 wt% deionized water. The effects of the concentration of SA-TiO_2 were investigated

Table 1: Photovoltaic performance of DSSCs using water-based TiO_2 nanofluids. Two-step method was used to manufacture the semiconductor on FTO substrate. Step one, the substrate was coated at 1500 rpm for 30 sec. Step two, the substrate was dried at 1000 rpm for 60 sec.

TiO_2 nanofluid (weight%)	Thickness (μm)	V_{oc} (mV)	J_{sc} (mA/cm^2)	FF	η (%)
BR-TiO_2 40 wt%	4	708	6.40	0.68	3.08
SA-TiO_2 14 wt% and BR-TiO_2 26 wt%	3.5	692	5.93	0.65	2.67
SA-TiO_2 20 wt% and BR-TiO_2 20 wt%	4.5	709	9.31	0.64	4.22
SA-TiO_2 34 wt% and BR-TiO_2 6 wt%	5.5	684	9.95	0.61	4.15

Table 2: Photovoltaic performance of DSSCs using water-based TiO_2 nanofluids. Two different spin coating strategies were used to manufacture the semiconductor on FTO substrate.

TiO_2 nanofluid (weight%)	Spin coating strategy	Thickness (μm)	V_{oc} (mV)	J_{sc} (mA/cm^2)	FF	η (%)
SA-TiO_2 20 wt% and BR-TiO_2 20 wt%	500 rpm for 250 sec	6	700	10.2	0.68	4.86
SA-TiO_2 20 wt% and BR-TiO_2 20 wt%	Step 1: 1500 rpm for 30 sec Step 2: 1000 rpm for 60 sec	4.5	709	9.31	0.64	4.22

Table 3: Photovoltaic performance of DSSCs using water-based TiO_2 nanofluids. Two different sintering strategies were used to manufacture semiconductor on FTO substrate. Sintering strategy: (i) sintered at 500°C for 60 minutes. The temperature raised and decreased to 500°C with speed of 100 rpm per hour and (ii) the temperature raised to 500°C with speed of 100 rpm per 6 min and decreased to ambient temp. with speed of 100 rpm per hour.

TiO_2 nanofluid (weight%)	Sintering strategy	Thickness (μm)	V_{oc} (mV)	J_{sc} (mA/cm^2)	FF	η (%)
SA-TiO_2 20 wt% and BR-TiO_2 20 wt%	(i)	4.5	709	9.31	0.64	4.22
SA-TiO_2 20 wt% and BR-TiO_2 20 wt%	(ii)	4	680	9.58	0.62	4.04

on performance of semiconductor while the total concentration of TiO_2 was kept constant at 40 wt%. The nanofluid was deposited on FTO substrate, and then the deposited nanoparticles were sintered to produce the semiconductor. It was observed that the efficiency of solar cell increased with concentration of SA-TiO_2. The solar cell had a maximum efficiency at concentration of 20 wt% SA-TiO_2 and 20 wt% BR-TiO_2. As concentration of SA-TiO_2 increased further, the efficiency of solar cell decreased. For all above cases, two-step method was used to coat the FTO substrate. Substrate was spin coated, using 1500 rpm for 30 sec, and then the dispersed nanofluid was dried at 1000 rpm for 60 sec subsequently.

To understand the effects of coating strategy, a mixture of 60 wt% water, 20 wt% SA-TiO_2, and 20 wt% BR-TiO_2 was used to build the semiconductor on FTO substrate using two different coating strategies. The photovoltaic performance in Table 2 clearly shows that coating strategy has a significant effect on solar cell efficiency. The experimental results indicated that the solar cell efficiency enhances with thickness of the semiconductor for given conditions. As thickness of semiconductor increases, the interfacial area for dye adsorption increases to improve the photocurrent.

Table 3 shows the photovoltaic performance of DSSCs compared with two different sintering strategies. The longer sintering time (5 hours for the raising temperature) leads to the V_{oc} increase (~29 mV). It is likely that a better diffusion between nanoparticles and more crystal growth leads to the reduction of grain boundaries of TiO_2 and consequently suppression of recombination phenomenon which can be seen with reduction of V_{oc}. It is also important that the electrode with 20 wt% SA-TiO_2 and 20% BR-TiO_2 can show relatively higher V_{oc}. These results indicated that the recombination phenomenon is not significant. In principle, the recombination phenomenon is suppressed with less grain boundary of TiO_2 particle [23]. Therefore, such an unwanted reaction can be reduced at an optimal TiO_2 mixture that enables to decrease the grain boundary of TiO_2 domain. The sintering of the SA-TiO_2 (anatase) accelerates the interparticle crystal growth. This may decrease the grain boundary, and consequently, the electron transport efficiency and V_{oc} increase. Contrarily, the 85 wt% of SA-TiO_2 had lower V_{oc}. This is probably due to the increased recombination reaction sites with increasing the surface area of nanostructured anatase TiO_2.

It was also found that the efficiency of solar cell is enhanced up to 4.86%, by modifying characteristics of nanofluid, spin coating, and sintering strategies. The conversion efficiency achieved by using D205 dye molecules is comparable with indoline dyes (3.39–5.46%), reported by our group, in which a high-performance TiO_2 paste (PST-18NR) was adapted for the device assembly [17]. Furthermore, such a respectable performance was achieved without a commonly used $TiCl_4$ treatment (for making better contacts between TiO_2 particles and/or, TiO_2 particle, and FTO) in this work, suggesting that our submicron-scale TiO_2 particles can offer favorable electron transport in indoline-based DSSCs.

4. Conclusions

We present the effects of water-based TiO_2 nanofluids on the improved photoanode performance of indoline-based DSSCs.

A mixture of SA-TiO_2 and 3D BR-TiO_2 particles was used to optimize the DSSC performance. It was suggested that the overall solution deposition process of TiO_2 photoelectrodes has significant potential in further development of high-efficiency DSSCs, in which numerous 3D TiO_2 particle morphologies can be applied to boost the power conversion efficiency. Most importantly, our water-based nanofluid is expected to open up new synthetic routes of the semiconducting porous photoelectrodes with anisotropic rod-shaped morphologies, whose environmentally friendly production is beneficial for realizing cost-effective DSSCs.

Conflicts of Interest

The authors declare that they have no conflicts of interest.

Acknowledgments

This work is partially supported by JSPS KAKENHI Grant no. 15K05664 and The Strategic Core Technology Advancement Program, "Supporting Industry Program."

References

[1] O. Ostroverkhova, "Organic optoelectronic materials: mechanisms and applications," *Chemical Reviews*, vol. 116, pp. 13279–13412, 2016.

[2] M. Grätzel, "Recent advances in sensitized mesoscopic solar cells," *Accounts of Chemical Research*, vol. 42, pp. 1788–1798, 2009.

[3] Y. Bai, I. Mora-Seró, F. D. Angelis, J. Bisquert, and P. Wang, "Titanium dioxide nanomaterials for photovoltaic applications," *Chemical Reviews*, vol. 114, pp. 10095–10130, 2014.

[4] X. Wang, Z. Li, J. Shi, and Y. Yu, "One-dimensional titanium dioxide nanomaterials: nanowires, nanorods, and nanobelts," *Chemical Reviews*, vol. 114, pp. 9346–9384, 2014.

[5] W. Q. Wu, Y. F. Xu, H. S. Rao, C. Y. Su, and D. B. Kuang, "Multistack integration of three-dimensional hyperbranched anatase titania architectures for high-efficiency dye-sensitized solar cells," *Journal of the American Chemical Society*, vol. 136, pp. 6437–6445, 2014.

[6] P. Roy, S. Berger, and P. Schmuki, "TiO2 nanotubes: synthesis and applications," *Angewandte Chemie, International Edition*, vol. 50, pp. 2904–2939, 2011.

[7] J. M. Kroon, N. J. Bakker, H. J. P. Smit et al., "Nanocrystalline dye-sensitized solar cells having maximum performance," *Progress in Photovoltaics: Research and Applications*, vol. 15, pp. 1–18, 2007.

[8] K. Manseki, K. Saka, M. Matsui, S. Vafaei, and T. Sugiura, "Structure identification of Ti(IV) clusters in low temperature TiO_2 crystallization: creating high-surface area brush-shaped rutile TiO_2," *CrystEngComm*, 2017.

[9] S. Vafaei, D. Wen, and T. Borca-Tasciuc, "Nanofluid surface wettability through asymptotic contact angle," *Langmuir*, vol. 27, pp. 2211–2218, 2011.

[10] S. Vafaei, A. Purkayastha, A. Jain, G. Ramanath, and T. Borca-Tasciuc, "The effect of nanoparticles on the liquid–gas surface tension of Bi2Te3 nanofluids," *Nanotechnology*, vol. 20, article 185702, 2009.

[11] S. Vafaei, T. Borca-Tasciuc, M. Z. Podowski, A. Purkayastha, G. Ramanath, and P. M. Ajayan, "Effect of nanoparticles on sessile droplet contact angle," *Nanotechnology*, vol. 17, pp. 2523–2527, 2006.

[12] S. Vafaei, C. Tuck, R. Wildman, and I. Ashcroft, "Surface microstructuring to modify wettability for 3D printing of nano-filled inks," *Chemical Engineering Research and Design*, vol. 109, pp. 414–420, 2016.

[13] S. Vafaei, K. Chinnathambi, and T. Borca-Tasciuc, "Liquid–gas surface tension voltage dependence during electrowetting on dielectric testing of water and 5–90 nm gold nanofluids," *Journal of Colloid and Interface Science*, vol. 490, pp. 797–801, 2017.

[14] S. Vafaei and M. Z. Podowski, "Analysis of the relationship between liquid droplet size and contact angle," *Advances in Colloid and Interface Science*, vol. 113, pp. 133–146, 2005.

[15] S. Vafaei and D. Wen, "Modification of the Young–Laplace equation and prediction of bubble interface in the presence of nanoparticles," *Advances in Colloid and Interface Science*, vol. 225, pp. 1–15, 2015.

[16] S. Vafaei and D. Wen, "The effect of gold nanoparticles on the spreading of triple line," *Microfluidics and Nanofluidics*, vol. 8, pp. 843–848, 2010.

[17] M. Matsui, N. Tanaka, Y. Kubota et al., "Long-term stability of novel double rhodanine indoline dyes having one and two anchor carboxyl group (s) in dye-sensitized solar cells," *RSC Advances*, vol. 6, pp. 33111–33119, 2016.

[18] S. Ito, S. M. Zakeeruddin, R. Humphry-Baker et al., "High-efficiency organic-dye-sensitized solar cells controlled by nanocrystalline-TiO2 electrode thickness," *Advanced Materials*, vol. 18, pp. 1202–1205, 2006.

[19] S. Vafaei, "Nanofluid pool boiling heat transfer phenomenon," *Powder Technology*, vol. 277, pp. 181–192, 2015.

[20] S. Vafaei and T. Borca-Tasciuc, "Role of nanoparticles on nanofluid boiling phenomenon: nanoparticle deposition," *Chemical Engineering Research and Design*, vol. 92, pp. 842–856, 2014.

[21] S. Vafaei and D. Wen, "Critical heat flux of nanofluids inside a single microchannel: experiments and correlations," *Chemical Engineering Research and Design*, vol. 92, pp. 2339–2351, 2014.

[22] S. Vafaei and D. Wen, "Flow boiling heat transfer of alumina nanofluids in single microchannels and the roles of nanoparticles," *Journal of Nanoparticle Research*, vol. 13, pp. 1063–1073, 2011.

[23] J. Jiu, S. Isoda, F. Wang, and M. Adachi, "Dye-sensitized solar cells based on a single-crystalline TiO2 nanorod film," *The Journal of Physical Chemistry B*, vol. 110, pp. 2087–2092, 2006.